JOURNAL OF COMPUTATIONAL PHYSICS 26, 379–389 (1978)

# Finite Hybrid Elements to Compute the Ideal Magnetohydrodynamic Spectrum of an Axisymmetric Plasma

R. GRUBER

*Centre de Recherches en Physique des Plasmas, École Polytechnique Fédérale de Lausanne, CH-1007 Lausanne, Switzerland*

Received September 27, 1976; revised February 10, 1977

We propose a new method, the "finite hybrid elements," to compute the ideal *MHD* spectrum of an axisymmetric plasma. This approach is well suited to calculate even weakly unstable internal modes of a tokamak-like plasma. It consists in extending the number of variables in the Lagrangian by considering the derivatives of the displacements as additional variables and then introducing auxiliary constraints between the variables and their derivatives. The discretisation of the problem by extremizing the Lagrangian leads to an underestimation of the potential energy, contrary to the standard finite element method. The lowest order solution makes each term of the Lagrangian piecewise constant on each mesh cell which facilitates the use of numerical equilibria. The results of test cases show a considerable improvement over the regular finite element method.

## 1. INTRODUCTION

In a previous paper {1} we proposed the regular finite elements as a method to find the ideal MHD spectrum of axisymmetric plasmas. The idea was to choose different basis functions for different vector components, such that the incompressibility condition $\nabla \cdot \xi = 0$ *can* be identically satisfied if necessary. For a straight elliptical geometry, we have shown that the fast growing kink modes are well reproduced with a reasonable number of mesh cells. However, in a "low-$\beta$" tokamak-like plasma, the internal modes, with growth rates which are about two orders of magnitude smaller, are strongly stabilized due to a poor representation of the $\mathbf{B} \cdot \nabla$-operator. This happens already in the straight circular case and it becomes worse with an elliptical cross-section.

In this paper, we apply a completely different method for which we propose the name "finite hybrid elements". The basic idea is to consider the vector *components* and their *derivatives* as *distinct variables* which are constrained only at specific points in each mesh cell. The basis functions are chosen in such a way that each term in the Lagrangian has the same functional dependence. To test the method we apply it to a cylindrical geometry. However, applications to axisymmetric geometries have successfully been done {8}. In order to present the method, we restrict ourselves to straight geometries. No pollution {2} has been observed. The weakly growing modes are obtained already with few points, even in situations where it was impossible to find



0021-9991/78/0263-0379$02.00/0

them with the regular finite elements expansion. A shift of the spectrum towards higher $q$-values is observed. This shift shows a quadratic convergence behavior when varying the number of azimuthal intervals. In a full two-dimensional, straight elliptical test case, we eliminate the shift and find a 4th order superconvergence of the eigenvalue which is approached from below!

In conclusion, we have found that it is not possible to brutishly apply the standard finite element method to the Lagrangian. The unstable modes are nearly incompressible and the internal modes are characterized by the operator $\mathbf{B} \cdot \nabla$ vanishing exactly on a singular surface. To correctly represent all the unstable modes, it is necessary to respect these features by an adequate approximation scheme. The finite hybrid element method, proposed here as the ultimate solution, may not be the only possibility, but it has shown computational advantages. It is well adapted to the study of numerically determined equilibria, and it is easy to implement.

## 2. The Problem

The variation of the Lagrangian {3} in ideal MHD can be written symbolically as

$$\delta L\left(\frac{\partial X}{\partial \chi}, X, \frac{\partial X}{\partial \psi}, \frac{\partial Y}{\partial \chi}, Y, \frac{\partial Z}{\partial \chi}, Z\right) = 0 \tag{1}$$

where $X$, $Y$ and $Z$ are related to the displacement components $\xi_\psi$, $\xi_z$ and $\xi_\chi$ by {3}

$$(X, Y, Z) = (B_p \xi_\psi, \xi_z, \xi_\chi / B_P). \tag{2}$$

The independent variables $\psi$, $z$ and $\chi$ are orthogonal and denote the radial, the ignorable axial and the azimuthal directions, respectively. $B_P$ denotes the poloidal magnetic field and $J$ is the Jacobian. The most important feature of the variational form, Eq. (1), is that there is only one radial derivative which acts on the radial component $X$.

We intend to study only internal modes which numerically are difficult to calculate {1}. In order to specifically treat these modes, we put the conducting wall right on the plasma surface. The boundary condition thenbecomes

$$X(\psi = \psi_s, \chi) = 0. \tag{3}$$

The subscript $s$ always denotes the plasma surface.

In addition we have to prescribe a regularity condition on the magnetic axis,

$$X(\psi = 0, \chi) = 0 \tag{4}$$

and the periodicity conditions in $\chi$ give

$$\begin{aligned} X(\psi, \chi = 0) &= X(\psi, \chi = 2\pi) \\ Y(\psi, \chi = 0) &= Y(\psi, \chi = 2\pi) \\ Z(\psi, \chi = 0) &= Z(\psi, \chi = 2\pi). \end{aligned} \tag{5}$$

Equation (1), together with the constraints (3), (4) and (5), completely define the problem.

When we treated Eq. (1) by a regular finite element expansion {1} we found that we were not able to fulfil the condition

$$\mathbf{B} \cdot \nabla(J \cdot f) = \frac{\partial f}{\partial \chi} + ikJB_z f = 0 \tag{6}$$

on a singular surface. Here $B_z$ denotes the longitudinal magnetic field, and $k$ is the longitudinal wave number. $f$ can be either $X$, $Y$ or $Z$.

As a basically new idea, we look for a method where $(\partial f/\partial \chi)$ and $f$ have the same functional dependence. This can be obtained by Fourier analyzing the problem as previously done by Kerner et al. {4} and by the Princeton group {5}. The finite hybrid element expansion, as an alternative method, consists in expanding the function $f$ and its derivatives $(\partial f/\partial \chi)$ and $(\partial f/\partial \psi)$ by different basis functions. Instead of solving the problem (1) we solve

$$\delta L \left( \frac{\partial X^{(1)}}{\partial \chi}, X^{(2)}, \frac{\partial X^{(3)}}{\partial \psi}, \frac{\partial Y^{(1)}}{\partial \chi}, Y^{(2)}, \frac{\partial Z^{(1)}}{\partial \chi}, Z^{(2)} \right) = 0, \tag{7}$$

restricted by the evident identities

$$\begin{aligned} X^{(1)} &= X^{(2)} = X^{(3)} \\ Y^{(1)} &= Y^{(2)} \\ Z^{(1)} &= Z^{(2)}. \end{aligned} \tag{8}$$

The original problem is reobtained when the identities, Eqs. (8), are substituted back into Eq. (7). In our approach, however, we vary the Lagrangian over all 7 variables $X^{(1)}$, $X^{(2)}$, $X^{(3)}$, $Y^{(1)}$, $Y^{(2)}$, $Z^{(1)}$ and $Z^{(2)}$, and do not impose the identities in Eqs. (8) everywhere, but only on specific points in each mesh cell. To prepare the discretisation of the problem, we rewrite the constraits (8) in the equivalent forms

$$\begin{aligned} \lim_{\Delta \to 0} \frac{1}{\Delta} \int_{\Delta} (X^{(2)} - X^{(1)})\, d\tau = 0, \qquad & \forall \Delta \in \Omega \\ \lim_{\Delta \to 0} \frac{1}{\Delta} \int_{\Delta} (X^{(2)} - X^{(3)})\, d\tau = 0, \qquad & \forall \Delta \in \Omega \\ \lim_{\Delta \to 0} \frac{1}{\Delta} \int_{\Delta} (Y^{(2)} - Y^{(1)})\, d\tau = 0, \qquad & \forall \Delta \in \Omega \\ \lim_{\Delta \to 0} \frac{1}{\Delta} \int_{\Delta} (Z^{(2)} - Z^{(1)})\, d\tau = 0, \qquad & \forall \Delta \in \Omega \end{aligned} \tag{9}$$

where $\Omega$ denotes the plasma domain.

## 3. Discretisation

In order to discretise the problem we cover the domain $\Omega$ with a rectangular mesh $(N_\psi \times N_\chi)$ in $\psi$ and $\chi$. We want to use a finite element expansion of the variables $X^{(1)}, X^{(2)}, X^{(3)}, Y^{(1)}, Y^{(2)}, Z^{(1)}$ and $Z^{(2)}$ which satisfies two requirements:

— each argument in Eq. (7) has the same functional dependence on $\psi$ and $\chi$,

— the constraints (9) are satisfied when $\Delta$ is identified with the size of a mesh cell $\Delta_{ij}$, such that

$$\begin{aligned}
\frac{1}{\Delta_{ij}} \int_{\Delta_{ij}} (X^{(2)} - X^{(1)})\, d\psi\, d\chi = 0, \qquad \forall i, j \\
\frac{1}{\Delta_{ij}} \int_{\Delta_{ij}} (X^{(2)} - X^{(3)})\, d\psi\, d\chi = 0, \qquad \forall i, j \\
\frac{1}{\Delta_{ij}} \int_{\Delta_{ij}} (Y^{(2)} - Y^{(1)})\, d\psi\, d\chi = 0, \qquad \forall i, j \\
\frac{1}{\Delta_{ij}} \int_{\Delta_{ij}} (Z^{(2)} - Z^{(1)})\, d\psi\, d\chi = 0, \qquad \forall i, j
\end{aligned} \tag{10}$$

These conditions do not uniquely determine the elements, so that we still can choose the order. We make the simplest choice possible by requiring that each argument in Eq. (7) be constant on each mesh cell.

Calling $e_{i+\frac{1}{2},j}$ the basis functions for $X^{(1)}$, $Y^{(1)}$ and $Z^{(1)}$, $f_{i+\frac{1}{2},j+\frac{1}{2}}$ the basis functions for $X^{(2)}$, $Y^{(2)}$ and $Z^{(2)}$, and $g_{ij+\frac{1}{2}}$ as the basis functions for $X^{(3)}$, the expansion can be written:

$$\begin{aligned}
\begin{pmatrix} X \\ Y \\ Z \end{pmatrix}^{(1)} &= \sum_{i=0}^{N_\psi - 1} \sum_{j=0}^{N_\chi} \begin{pmatrix} X \\ Y \\ Z \end{pmatrix}^{(1)}_{i+\frac{1}{2}\, j} e_{i+\frac{1}{2}\, j} \\
\begin{pmatrix} X \\ Y \\ Z \end{pmatrix}^{(2)} &= \sum_{i=0}^{N_\psi - 1} \sum_{j=0}^{N_\chi - 1} \begin{pmatrix} X \\ Y \\ Z \end{pmatrix}^{(2)}_{i+\frac{1}{2}\, j+\frac{1}{2}} f_{i+\frac{1}{2}\, j+\frac{1}{2}} \\
X^{(3)} &= \sum_{i=0}^{N_\psi} \sum_{j=0}^{N_\chi - 1} X^{(3)}_{ij+\frac{1}{2}} g_{ij+\frac{1}{2}}\,,
\end{aligned} \tag{11}$$

where the position of the nodal values in a mesh cell are shown in Fig. 1 and the shape of the corresponding basis functions are shown in Fig. 2.

Note, that $e_{i+\frac{1}{2}j}(\chi)$ is a function linear in $\chi$ and piecewise constant in $\psi$. The $\chi$ derivative of such an element is piecewise constant. A similar roof function, linear in $\psi$ and constant in $\chi$, is used for $g_{ij+\frac{1}{2}}(\psi)$, such that the $\psi$ derivative be piecewise constant. The basis for $f_{i+\frac{1}{2}j+\frac{1}{2}}$ is piecewise constant. The first requirement is then satisfied.

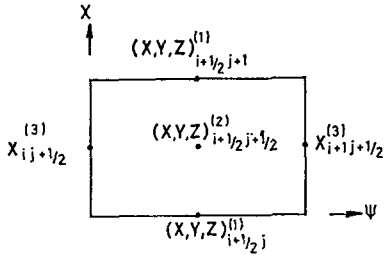


FIG. 1. Position of the nodal values in a mesh cell for the "finite hybrid elements."

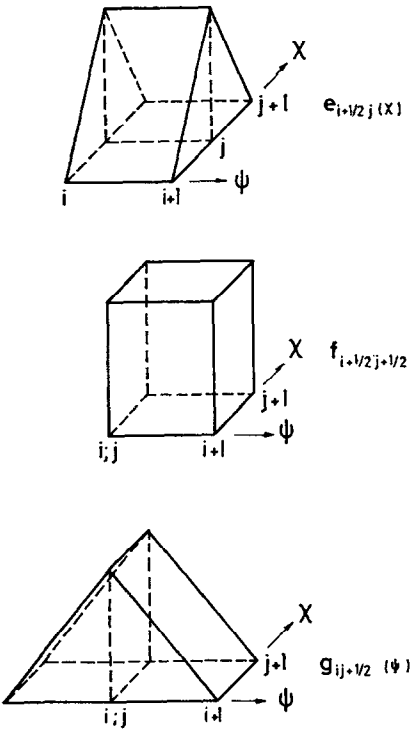


FIG. 2. Shape of the basis functions $e_{i+1/2\ j}(\chi)$ for the expansion of $X^{(1)}$, $Y^{(1)}$, and $Z^{(1)}$ of $f_{i+1/2\ j+1/2}$ for the expansion of $X^{(2)}$, $Y^{(2)}$ and $Z^{(2)}$ and of $g_{ij+1/2}(\psi)$ for the expansion of $X^{(3)}$.

Substituting the expansion (11) into the second requirements, Eq. (10), leads to the following relations:

$$X^{(2)}_{i+\frac{1}{2}\ j+\frac{1}{2}} = \frac{X^{(1)}_{i+\frac{1}{2}\ j} + X^{(1)}_{i+\frac{1}{2}\ j+1}}{2}$$

$$X^{(2)}_{i+\frac{1}{2}\ j+\frac{1}{2}} = \frac{X^{(3)}_{ij+\frac{1}{2}} + X^{(3)}_{i+1\ j+\frac{1}{2}}}{2} \tag{12}$$

$$Y^{(2)}_{i+\frac{1}{2}\,j+\frac{1}{2}} = \frac{Y^{(1)}_{i+\frac{1}{2}\,j} + Y^{(1)}_{i+\frac{1}{2}\,j+1}}{2}$$

$$Z^{(2)}_{i+\frac{1}{2}\,j+\frac{1}{2}} = \frac{Z^{(1)}_{i+\frac{1}{2}\,j} + Z^{(1)}_{i+\frac{1}{2}\,j+1}}{2}$$

Note that $X^{(1)}$, $X^{(2)}$ and $X^{(3)}$ are equal at the center of each mesh cell. The same is true for $Y^{(1)}$, $Y^{(2)}$ and $Z^{(1)}$, $Z^{(2)}$. Since in the Lagrangian, Eq. (7), all the functions and their derivatives are piecewise constant, the equilibrium is also taken piecewise constant. This is done by replacing the coefficients in the Lagrangian by their values at the center of each cell.

Equations (12) able us to eliminate $X^{(1)}$, $X^{(2)}$, $Y^{(2)}$ and $Z^{(2)}$. The remaining unknowns are then $X^{(3)}_{ij+\frac{1}{2}}$, $Y^{(1)}_{i+\frac{1}{2}\,j}$ and $Z^{(1)}_{i+\frac{1}{2}\,j}$. With this choice the boundary conditions (3, 4) take the simple form

$$\begin{aligned} X^{(3)}_{0\,j+\frac{1}{2}} &= 0 \\ X^{(3)}_{N_\psi j+\frac{1}{2}} &= 0 \end{aligned} \qquad 0 \leqslant j \leqslant N_\chi - 1 \tag{13}$$

and the periodicity conditions (5) in $\chi$ yield

$$\begin{aligned} X^{(3)}_{i+\frac{1}{2}\,0} &= X^{(3)}_{i+\frac{1}{2}\,N_\chi} \\ Y^{(1)}_{i+\frac{1}{2}\,0} &= Y^{(1)}_{i+\frac{1}{2}\,N_\chi} \qquad 0 \leqslant i \leqslant N_\psi - 1 \\ Z^{(1)}_{i+\frac{1}{2}\,0} &= Z^{(1)}_{i+\frac{1}{2}\,N_\chi} \end{aligned} \tag{14}$$

We can now verify that

$$\nabla \cdot \xi = \frac{\partial X^{(3)}}{\partial \psi} + ikY^{(2)} + \frac{\partial Z^{(1)}}{\partial \chi}$$

and

$$\mathbf{B} \cdot \Delta JX = \frac{\partial X^{(1)}}{\partial \chi} + ikJB_z X^{(2)},$$

being piecewise constant, can indeed vanish over each mesh cell.

Compared with the usual finite element method {1} the additional freedom introduced by the enlargement of the functional space leads to lower energy level. This helps to separate better the weakly growing unstable mode from the stable continuous region.

The variational form given by Eq. (7) contains $7N_\psi N_\chi + 3N_\psi + N_\chi$ variables. The regularity condition (4) fixes $N_\chi$ variables. For a wall constrained plasma, the boundary condition (3) fixes also $N_\chi$ variables. The periodicity conditions, Eqs. (14), eliminate $3N_\psi$ unknowns and the identities (12) reduce the number of unknowns by $4N_\psi N_\chi$. For the case with a vacuum region there remain $3N_\psi N_\chi$ nodal values and for a wall constrained case there are $3N_\psi N_\chi - N_\chi$ unknowns.

A code has been written which uses this method. Various tests have been run. The results are compared with results obtained using our 1-D code and a regular finite element expansion {1}.

## 4. Application to the Cylindrical Case and Comparison with Regular Elements

The first test case consists of a straight circular plasma column of constant density $\rho$, traversed by a longitudinal current of constant intensity $j$ and imbedded in a homogeneous field $B_z$. A rigid boundary is placed right on the plasma surface. Because of the symmetry, the spectrum can be computed for each azimuthal wave number $m$ by one-dimensional code THALIA {6}. We consider the case $m = 1$ and $m = 2$. We normalize all our calculations to the Alfven speed, i.e., on $\omega_a{}^2 = k^2 B_z{}^2/\rho R^2 = j^2/4\rho$, where $R$ is the radius of the plasma surface. The homogeneous current density was chosen to be $j = 0.4\, B_z/R$. The number of radial intervals was taken to be $N_\psi = 12$ throughout the whole $m = 1$ calculations. For $m = 2$, $N_\psi$ varies. For simplicity we always choose the number of azimuthal intervals $N_\chi$ to be $2N_\psi$ in the full range $0 \leqslant \chi \leqslant 2\pi$. Making use of the symmetry, the code only uses half the number of azimuthal intervals in the range $0 \leqslant \chi \leqslant \pi$. Figures 3a-b show the results for the

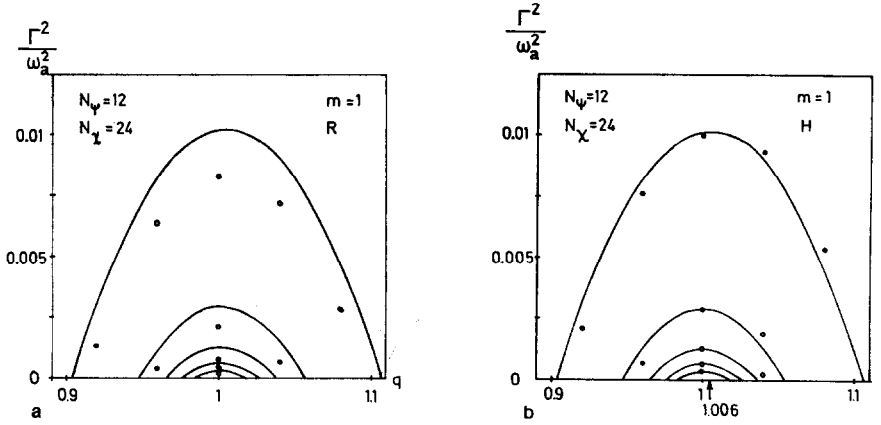


FIG. 3. Comparison of the first 5 fundamental radial modes of the wall constrained circular test case, using: (a) regular finite elements {1}, (b) finite hybrid elements with a piecewise constant equilibrium. The solid lines denote the results obtained with THALIA {6} which can be considered as exact.

$m = 1$ case. The square of the growth rates $\Gamma^2$ of the internal modes is plotted versus the safety factor $q \equiv krB_z/B_p = 5kR$. The solid curves represent the results obtained with the 1-D code {6}. The small circles are results obtained with:

a) Regular finite elements as described in {1}.

b) Finite hybrid elements.

The results in Fig. 3a show a rather large discrepancy with the 1-D results. In both cases the spectra are not polluted {2}. This can be seen by studying the unstable part of the spectrum at $q = 1$. Here, an infinite number of unstable fundamental modes should be observed. Numerically, this means that $N_\psi - 1$ modes are unstable when $N_\psi$ radial intervals are taken. Thus, at $q = 1$, with $N_\psi = 12$, one should find 11 unstable Alfven modes. It is surprising that one obtains 9 of them in the highly stabilized case (a). The stabilizing effect due to the coupling between the modes must therefore diminish for higher radial Alfven modes. From these results we expect that the coupling effect, observed in Fig. 3a, disappears when an infinite number of mesh cells are taken, e.g. no pollution. In case (b) only 8 unstable displacement vectors are found at $q = 1$. This comes from the fact that there is a shift of the growth rate curves by 0.6% towards higher $q$-values. When one counts the number of negative values of $\omega^2$ at $q = 1.006$, one finds all the 11 modes unstable. This shift of the whole spectrum depends mostly on the number of azimuthal intervals $N_\chi$ and little on $N_\psi$.

It is more difficult to calculate the unstable part of the $m = 2$ spectrum. The maximum growth rate is 8 times smaller than that obtained in the $m = 1$ spectrum, and the eigenfunction varies twice as rapidly in the angular direction. No unstable modes are found in this case with the regular finite elements method, even when 20 azimuthal intervals are taken in half the range ($N_\chi = 40$). Using finite hybrid elements, however, we obtain, with high accuracy, the whole unstable part of the spectrum as shown in Fig. 4. This shift towards higher $q$-values is more pronounced for a given number of mesh points. At $q = 2.017$, for example, we again find that all 11 fundamental modes are unstable! The cross at the upper right hand corner of Fig. 4 at $q = 2.11$ is the maximum value of $\Gamma^2$ obtained when taking only $N_\chi = 16$ azimuthal intervals. This value differs only by 5% from the maximum obtained with the 1-D

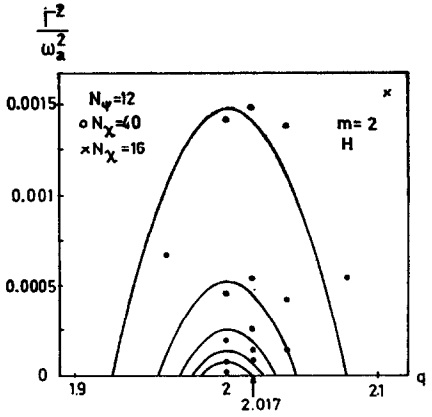


FIG. 4. Unstable part of the $m = 2$ spectrum of the wall constrained cylindrical test case, $kR = 0.2$. The solid curves represent the "exact" 1-D results. The small circles are the results of the 2-D calculations performed with the finite hybrid element method using a piecewise constant equilibrium, $N_\chi = 40$. The cross at the upper right hand corner at $q = 2.11$ is the maximum of the most unstable mode obtained with $N_\chi = 16$. No unstable modes are obtained with regular finite elements.

code. Note, that the maximum growth rate is over-estimated. This can never happen with regular finite elements, where one always approaches the most unstable mode from the stable side.

Let us now study the dependence of the shift as a function of the number of azimuthal intervals. The relative shift in $q$ as a function of $1/N_x^2$ is shown in Fig. 5 for $m = 2$. The straight line corresponds to a quadratic convergence of the shifted discretised spectrum. The convergence is to the "extact" 1-D result ($N_x \to \infty$).

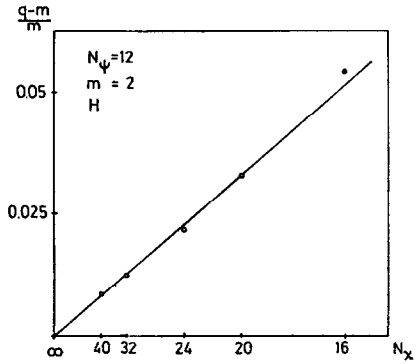


FIG. 5. Relative shift $(q - m)/m$ of the spectrum calculated with finite hybrid elements and a piecewise constant equilibrium versus $1/N_x^2$. The straight line corresponds to a quadratic convergence.

## 5. Straight Elliptical Test Case

As a second test, we consider a full two-dimensional case, the Gajewski equilibrium. It consists of a straight elliptical plasma column imbedded in a uniform magnetic field $B_z$. The mass density $\rho$ and the longitudinal current density $j$ are chosen constant. The surfaces of constant magnetic flux $\psi$ are similar ellipses. We denote by $\epsilon$ the ratio of the large axis to the small axis. The frequency is normalized to $\omega_a^2 = \epsilon^2 j^2/\rho(1 + \epsilon^2)^2$. This equilibrium is the same as considered by Dewar et al. {7}. The results have all been obtained with the current density fixed at $j = 0.4B_z/R$ and $\epsilon = 1.5$.

The growth rate of the most unstable mode has the same kind of dependence on $q$ as shown in Figs. 3 and 4. The value of $k$ which corresponds to the maximum growth rate varies with $N_x$. Figure 6 shows a plot of the maxium value of the growth rate squared $\Gamma^2$ versus $N_x^{-4}$. The fact that the points lie on a straight line means a 4th order superconvergence for $\Gamma^2$ as a function of $N_x$. This is surprising, since a quadratic convergence was expected from the order of the elements. Note, that throughout the whole range of $N_x$ studied, $\Gamma^2$ varies only by 4 %! In our previous paper {1} we made the same convergence study with regular finite elements for the same mode. There we did not find any evident quadratic convergence behavior even when taking up to 48 azimuthal intervals.

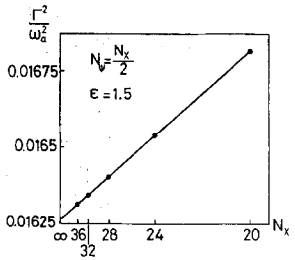


FIG. 6. Convergence study of the maximum growth rate as a function of $1/N_x^4$ for the elliptical test case, $\epsilon = 1.5$. The shift of $\Gamma^2(q)$ towards higher $q$-values has been taken into account. The straight line denotes a 4th order superconvergence.

These results show that the finite hybrid element method can indeed reproduce the weakly growing internal modes with only a few mesh cells. The shift in $q$ of the spectrum is not important as long as the characteristic features of the spectrum are well reproduced, namely the growth rates and the eigenfunctions.

## 6. CONCLUSIONS

We have proposed a new method for which we propose the name "finite hybrid element", to calculate the ideal 2-D MHD spectrum. The idea of the method is to choose a representation such that each term of the variational form has the same functional dependence and thus, exact cancelation between terms *can* occur. The method has been applied to straight circular and straight elliptical geometries. It has shown an impressive improvement over previous results obtained with regular finite elements. In all the fixed boundary cases which have been studied, we have found a 4th order superconvergence, when the shift towards higher $q$-values is eliminated.

From the technical point of view this method has advantages compared to the regular finite elements:

— The sizes of the matrices are smaller for the same number of mesh cells.

— The integration is trivial since all terms in the Lagrangian are piecewise constant.

— The method is particularly well suited for the stability calculation of numerically determined equilibria.

Since the completion of this work the code is being extended to deal with any axisymmetric toroidal configuration {8}. Among the new features, let us mention the inclusion of the vacuum region, a non-orthogonal coordinate system and an interface which allows numerical equilibrium to be used as input. We think that our finite hybrid element code will be a very powerful tool to study the ideal MHD instabilities of axisymmetric toroidal plasmas.

## ACKNOWLEDGMENTS

The author is greatfully indebted to Dr. D. Berger, Prof. Dr. J. Descloux, Dr. J. Rappaz and Prof. Dr. F. Troyon for their stimulating discussions, helpful suggestions and critical comments. He would also like to thank the staff of our computing center for their helpful support.

This work was supported by the Swiss National Science Foundation.

## REFERENCES

1. D. BERGER, R. GRUBER, AND F. TROYON, *Comput. Phys. Comm.* **11** (1976), 313.
2. J. RAPPAZ, Ph.D. Thesis, Lausanne, 1976. J. RAPPAZ, *Numer. Math.* **28** (1977), 15.
3. C. MERCIER, *Nucl. Fusion* **1**, 47 (1960).
4. W. KERNER, H. TASSO, Tokyo (1975), IAEA-CN-33/A13-1, 475; W. KERNER, PPPL report MATT-1229 (1976).
5. R. C. GRIMM, J. M. GREENE, J. L. JOHNSON, *in* "Method of Computational Physics" edited by (B. Alder, S. Fernbach, J. Killeen, and M. Rotenberg, Ed.), Vol. 16, Chap. 4, Academic Press, New York.
6. K. APPERT, D. BERGER, R. GRUBER, F. TROYON, K. V. ROBERTS, *Comput. Phys. Comm.* **10** (1975), 11.
7. R. L. DEWAR, R. C. GRIMM, J. L. JOHNSON, E. A. FRIEMAN, J. M. GREENE, P. H. RUTHERFORD, *Phys. Fluids* **17** (1974), 930.
8. D. BERGER, R. GRUBER, AND F. TROYON, paper C3, *in* "Proc. of the 2nd Europ. Conf. on Comp. Phys., Garching, 1976. "